micromachines

MDPI

Article

Enhanced Red Emission from Amorphous Silicon Carbide Films via Nitrogen Doping

Guangxu Chen, Sibin Chen, Zewen Lin, Rui Huang * and Yanqing Guo *

School of Materials Science and Engineering, Hanshan Normal University, Chaozhou 521041, China
* Correspondence: rhuang@hstc.edu.cn (R.H.); yqguo126@126.com (Y.G.)

Abstract: The enhanced red photoluminescence (PL) from Si-rich amorphous silicon carbide (a-SiC_x) films was analyzed in this study using nitrogen doping. The increase in nitrogen doping concentration in films results in the significant enhancement of PL intensity by more than three times. The structure and bonding configuration of films were investigated using Raman and Fourier transform infrared absorption spectroscopies, respectively. The PL and analysis results of bonding configurations of films suggested that the enhancement of red PL is mainly caused by the reduction in nonradiative recombination centers as a result of the weak Si–Si bonds substituted by Si–N bonds.

Keywords: photoluminescence; optical properties; nitrogen; SiCx

Citation: Chen, G.; Chen, S.; Lin, Z.; Huang, R.; Guo, Y. Enhanced Red Emission from Amorphous Silicon Carbide Films via Nitrogen Doping. *Micromachines* **2022**, *13*, 2043. https://doi.org/10.3390/mi13122043

Academic Editor: Hieu Pham Trung Nguyen

Received: 20 October 2022
Accepted: 20 November 2022
Published: 22 November 2022

1. Introduction

Efficient Si-based light sources are indispensable components for realizing Si-based monolithic optoelectronic integrated circuits. Silicon-based materials, such as silicon oxide (SiO_x), silicon nitride (SiN_x), silicon carbine (SiC_x), and silicon oxycarbide (SiC_xO_y), have been extensively investigated over the past decade to obtain efficient Si-based light sources [1–10]. However, light emission efficiency is still very low and commercial applications are difficult to meet. The low emission efficiency is mainly limited by the strongly nonradiative recombination originating from defects and low carrier injection efficiency [11]. Compared with the wide bandgap of SiO_2 and SiN_x, SiC_x features a smaller bandgap, which is more conducive to carrier injection and achieving electroluminescence at lower driving voltages in SiC_x-based light-emitting devices [5,12]. Although SiC_x possesses these advantages, research of its luminescence is still progressing slowly due to the strong nonradiative recombination derived from band tails and defect states in SiC_x induced by its structural disorder. In order to reduce nonradiative recombination, hydrogen treatment is often used to passivate defective states and improve structural order by etching weak Si–Si bonds [13]. However, the hydrogen used for passivation will fall off at high temperatures and lead to the recovery of defective states. Therefore, the regulation of defective states has become a key process for obtaining efficient SiC-based devices with suppressed nonradiative recombination centers. In previous research, the passivation of nitrogen on the Si nanocrystals surface was found to effectively increase the probability of radiative recombination [14]. Li et al. reported surface nitrogen-capped Si NPs with PL efficiency up to 90% at wavelength of 560 nm. However, up to now, there is no report on the effect of nitrogen passivation on the luminescent properties of SiC_x films [14].

In this study, the red luminescent Si-rich a-SiC_x films doped with N were fabricated using very high-frequency plasma-enhanced chemical vapor deposition (VHF-PECVD). The increase in nitrogen doping concentration in films significantly improves red light emission by more than three times. The enhanced red PL is discussed, which is mainly caused by the reduction in nonradiative recombination centers as a result of the weak Si–Si bonds substituted by Si–N bonds.

2. Experimental Details

Amorphous Si-rich a-SiC_x films doped with N were prepared via very high frequency plasma-enhanced chemical vapor deposition using SiH_4, CH_4, and NH_3 as reaction gas sources. These fabrications were carried out at a temperature of 250 °C. The RF power and the deposition pressure for the growth were kept at 30 W and 20 Pa, respectively. Flow rates of SiH_4 and CH_4 were maintained at 2.5 and 5 sccm (standard cubic centimeter per minute), respectively, while those of NH_3 varied from 0 sccm to 2 sccm. The PL spectra of the films were recorded by an Edinburgh FLS1000 fluorescence spectrometer equipped with a 450 W steady Xe lamp. The PL decay curves were measured by an Edinburgh FLS1000 spectrometer using a 372 nm picosecond laser (pulse width 44 ps, repetition rate = 20 MHz). The absorption spectra of the films were obtained with a Shimadzu UV-3600 spectrophotometer (Shimadzu UV-3600, Shimadzu Corporation, Kyoto, Japan). Microstructures of the films were evaluated using a Horiba LabRAM HR Evolution Raman spectrometer. Bonding structures were recorded via Fourier transform infrared absorption (FTIR) spectrometry (Shimadzu IR Pretige-21).

3. Results and Discussion

Figure 1 shows the PL spectra of thin films prepared at different NH_3 flow rates under an excitation wavelength of 325 nm. The prepared film without NH_3 only shows weak red light emission that peaks at ~780 nm. The emission peak position of the film changes minimally but the red light emission gradually intensifies with the addition of NH_3. The red light emission of the film is nearly three times stronger than that of the film prepared without NH_3 when the NH_3 flow rate increases to 2 sccm. This phenomenon is consistent with improvement of the photoluminescence properties in a-SiN_x films by the introduction of hydrogen [15]. Figure 2a,b reveal that the change in emission peak position and the full width at half maximum with the variation of the excitation wavelength is insignificant. This finding clearly features defect luminescence characteristics similar to those observed in defect-related luminescent Si-based materials, such as SiC_x and SiC_xO_y [6,8].

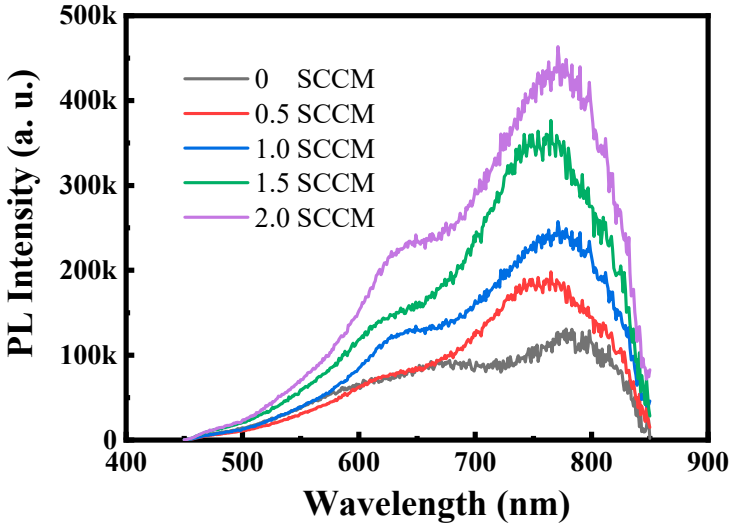

Figure 1. PL spectra of thin films prepared at different NH_3 flow rates under an excitation wavelength of 325 nm.

The microstructure of films was characterized using Raman scattering spectra to clarify the luminescence enhancement (Figure 3a). The Raman spectra show the typical features of a-Si vibration modes. The Raman peaks at around 150 cm^{-1} and 480 cm^{-1} are attributed to transverse acoustic (TA) and transverse optical (TO) phonon frequencies, respectively [16,17]. This finding indicates that amorphous silicon clusters exist but Si and SiC nanocrystals are absent in the films. Moreover, with an increased NH_3 flow rate, one

can see that the intensity ratio of the TA mode (150 cm^{-1}) to the TO mode (480 cm^{-1}) tends to decrease. These observations suggest a reduced short-range and medium-range disorder of the Si–Si_4 network [17]. This phenomenon is closely related to the increase in N content in the film. The weak Si–Si bond in the film will be gradually etched and replaced by the Si–N bond with the addition of N given that the Si–N bond energy (355 kJ/mol) is greater than the Si–Si bond energy (222 kJ/mol). It seems that the reduction in weak Si–Si bonds is responsible for the significant enhancement in red PL [18]. The surface morphology of the films was further revealed by atomic force microscopy (AFM) as shown in Figure 3b,c. The average RMS values for the films are around 20 nm. No obvious change can be observed in the surface morphology between the films prepared by different NH_3 flow rates. This ruled out the possibility that the enhanced PL was caused by the increasing light extraction from the films.

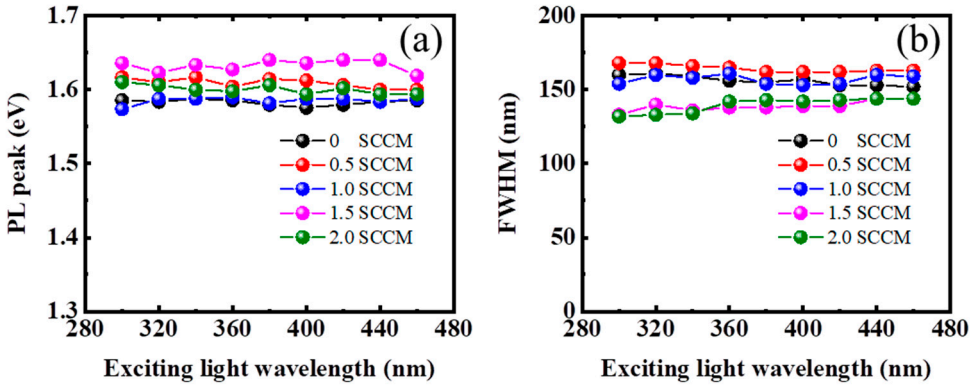

Figure 2. Emission peak position (**a**) and the full width at half maximum (**b**) with the variation of the excitation wavelength for the films prepared at different NH_3 flow rates, respectively.

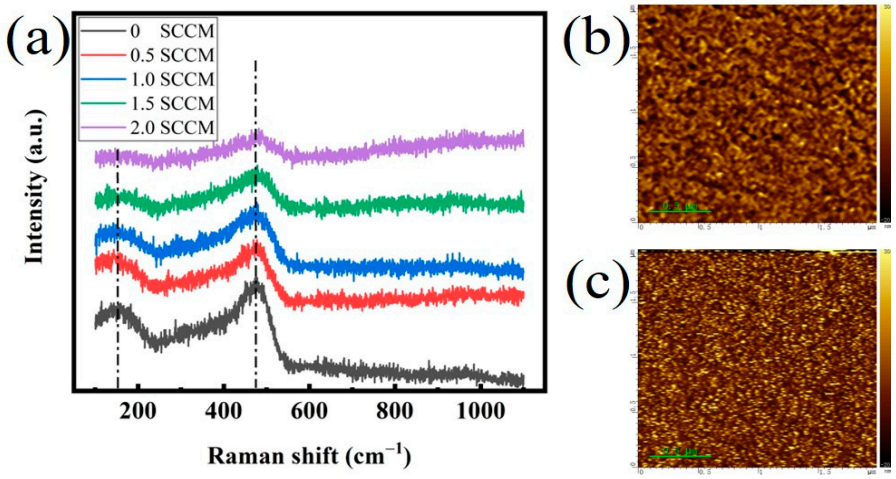

Figure 3. (**a**) Raman scattering spectra of the films prepared at different NH_3 flow rates, (**b**,**c**) atomic force microscopic images of the films prepared by different NH_3 flow rates of 1 sccm and 2 sccm, respectively.

Films were analyzed with an FTIR spectrometer to further explore the bonding configuration of films prepared with different NH_3 flow rates. The results are shown in Figure 4. The FTIR absorption spectrum for the film prepared without NH_3 mainly displays the following vibrational bands [6,16]: the absorption band at 640 cm^{-1} corresponds to the rocking vibration mode of SiH_n, the 780 cm^{-1} band is related to the stretching vibration mode of Si–C, the 1250 cm^{-1} band corresponds to the stretching vibration mode of Si–C, and the 2100 cm^{-1} band is attributed to the stretching vibration mode of H–Si–Si_3. The FTIR absorption spectrum clearly showed the feature of Si-rich SiC_x. One can see that

the rocking vibration mode of SiH_n at 640 cm^{-1} and the stretching vibration mode of H–Si–Si_3 at 2100 cm^{-1} gradually weaken with the increase in NH_3 flow rates. In contrast, the stretching vibration mode of Si–N appears and becomes intense with the addition of NH_3. With the NH_3 flow rate increasing from 0.5 to 2 sccm, the density of Si–N bond is estimated to be increased from 0.2 × 10^{22} cm^{-2} to 0.7 × 10^{22} according to the following equation [19]:

$$N = A \int \frac{\alpha(\omega)}{\omega} d\omega \quad (1)$$

where $\alpha(\omega)$ is the absorption coefficient, ω is the wave number of the corresponding absorption band, and A is equal to 6.3 × 10^{18} cm^{-2}, which is related to the absorption cross-section of the Si–N vibration mode. This finding strongly indicates that the weak Si–Si bond is gradually replaced by the Si–N bond with the continuous incorporation of N.

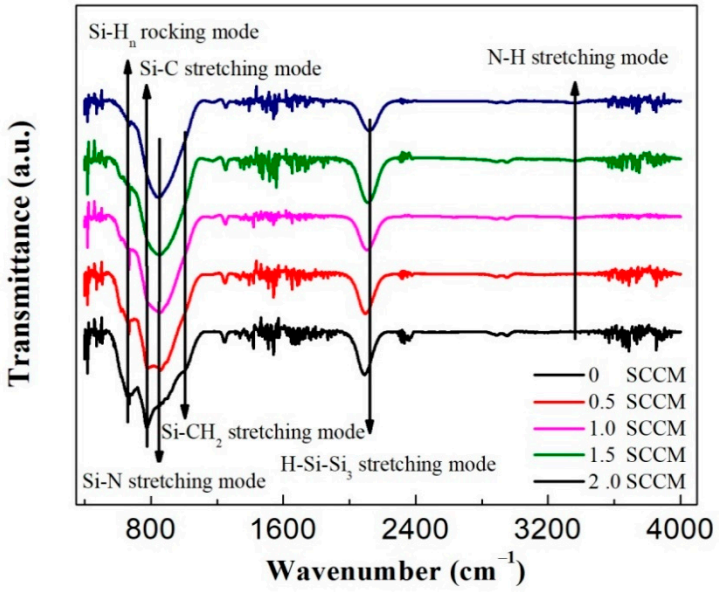

Figure 4. FTIR absorption spectra of the films prepared at different NH_3 flow rates.

Figure 5 shows the PL decay traces of films prepared under different NH_3 flow rates. The decay process in each case can be properly fitted with a biexponential function as follows:

$$I(t) = I_0 + A_1 \exp(\frac{-t}{\tau_1}) + A_2 \exp(\frac{-t}{\tau_2}) \quad (2)$$

where I_0 is the background level; τ_1 and τ_2 are the weight fraction and lifetime of each exponential decay component, respectively; and A_1 and A_2 are the corresponding amplitudes [20]. Thus, the average lifetime τ can be estimated as follows [20]:

$$\tau = (A_1 \times {\tau_1}^2 + A_2 \times {\tau_2}^2)/(A_1 \times \tau_1 + A_2 \times \tau_2) \quad (3)$$

Figure 5 shows that all measured films feature a fast dynamic decay with lifetimes of nanoseconds. Moreover, the PL lifetime gradually increases from 3.2 ns to 3.8 ns with the increase in NH_3 flow rates. The comparison of Figures 1 and 5 shows that the evolution of the PL lifetime with NH_3 flow rates is the same as that of PL intensity with NH_3 flow rates. This finding strongly indicates that the improved red light emission is due to the reduction in nonradiative recombination centers in the film. As demonstrated by Raman spectra in Figure 3, the amorphous silicon component in the film gradually decreases with the increase in the NH_3 flow rate. Meanwhile, the Si–N bond density increases with the increase in the NH_3 flow rate (Figure 4). These results clearly demonstrate that some Si–Si bonds are replaced by Si–N bonds. The weak Si–Si bond in the film will likely be gradually etched and replaced by the Si–N bond with the addition of N, given that the Si–N bond

energy (355 kJ/mol) is greater than the Si–Si bond energy (222 kJ/mol). The addition of nitrogen evidently reduces the nonradiative recombination centers in the film. Therefore, the increase in NH_3 flow rate increases the PL lifetime and significantly enhances red light emissions.

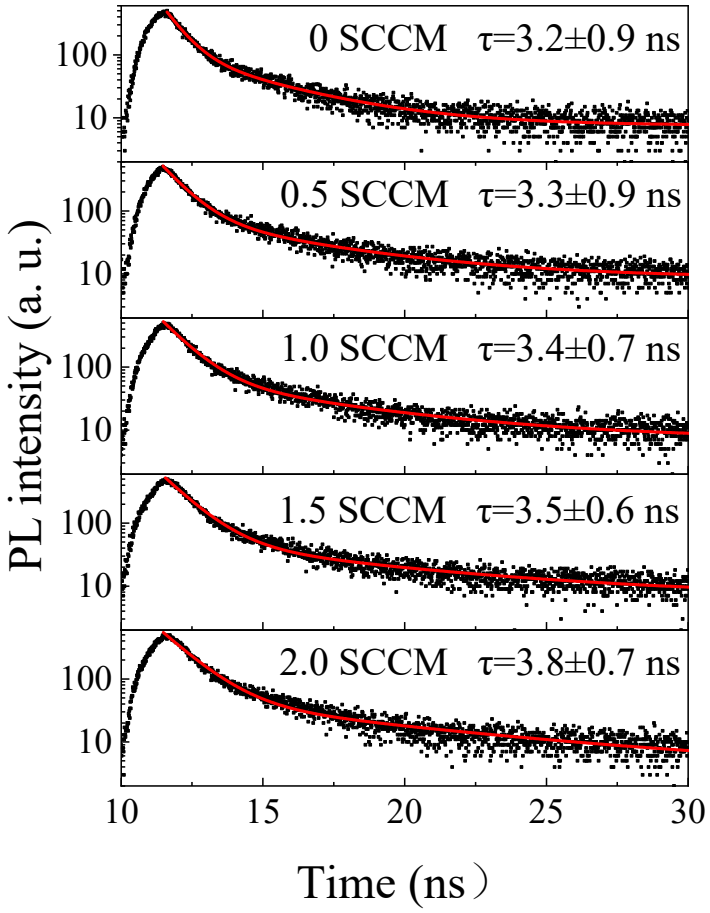

Figure 5. PL decay traces of the films prepared at different NH_3 flow rates.

4. Conclusions

Red luminescent Si-rich a-SiC_x films doped with N were fabricated using VHF-PECVD. The increase in nitrogen doping concentration in the films significantly improves red light emissions by more than three times. The PL results and analyses of bonding configurations of films demonstrated that the significant enhancement in red PL is caused by the effective reduction in nonradiative recombination centers from the reduction in weak Si–Si bonds substituted with Si–N bonds.

Author Contributions: G.C.: writing—original draft, investigation, formal analysis. S.C.: investigation, formal analysis. Z.L.: formal analysis. R.H.: writing—review and editing, investigation, formal analysis. Y.G.: investigation, formal analysis, writing—review and editing. All authors have read and agreed to the published version of the manuscript.

Funding: This work was supported by the Guangdong Basic and Applied Basic Research Foundation (2020A1515010432), Special Innovation Projects of Guangdong Provincial Department of Education (2020KTSCX076), Project of Educational Commission of Guangdong Province of China (2019KTSCX096, 2021ZDJS039), Special Funds for the Cultivation of Guangdong College Students' Scientific and Technological Innovation ("Climbing Program" Special Funds) (pdjh2021b0322).

Data Availability Statement: Data underlying the results presented in this paper are not publicly available at this time but may be obtained from the authors upon reasonable request.

Conflicts of Interest: The authors declare no conflict of interest.

References

1. Ni, Z.; Zhou, S.; Zhao, S.; Peng, W.; Yang, D.; Pi, X. Silicon nanocrystals: Unfading silicon materials for optoelectronics. *Mater. Sci. Eng. R Rep.* **2019**, *138*, 85–117. [CrossRef]
2. Nevin, W.A.; Yamagishi, H.; Yamaguchi, M.; Tawada, Y. Emission of blue light from hydrogenated amorphous silicon carbide. *Nature* **1994**, *368*, 529–531. [CrossRef]
3. Giorgis, F.; Mandracci, P.; Negro, L.D.; Mazzoleni, C.; Pavesi, L. Optical absorption and luminescence properties of wide-band gap amorphous silicon based alloys. *J. Non-Cryst. Solids* **2000**, *266–269*, 588–592. [CrossRef]
4. Fan, J.Y.; Wu, X.L.; Chu, P.K. Low-dimensional SiC nanostructures: Fabrication, luminescence, and electrical properties. *Prog. Mater. Sci.* **2006**, *51*, 983–1031. [CrossRef]
5. Vasin, A.V.; Kolesnik, S.P.; Konchits, A.A.; Rusavsky, A.V.; Lysenko, V.S.; Nazarov, A.N.; Ishikawa, Y.; Koshka, Y. Structure, paramagnetic defects and light-emission of carbon-rich *a*-SiC:H films. *J. Appl. Phys.* **2008**, *103*, 123710. [CrossRef]
6. Beke, D.; Szekrényes, Z.; Czigány, Z.; Kamarás, K.; Gali, Á. Dominant luminescence is not due to quantum confinement in molecular-sized silicon carbide nanocrystals. *Nanoscale* **2015**, *7*, 10982–10988. [CrossRef] [PubMed]
7. Wang, J.; Suendo, V.; Abramov, A.; Yu, L.; Roca i Cabarrocas, P. Strongly enhanced tunable photoluminescence in polymorphous silicon carbon thin films via excitation-transfer mechanism. *Appl. Phys. Lett.* **2010**, *97*, 221113. [CrossRef]
8. Lin, Z.; Huang, R.; Zhang, Y.; Song, J.; Li, H.; Guo, Y.; Song, C. Defect emission and optical gain in SiC_xO_y: H films. *ACS Appl. Mat. Interfaces* **2017**, *9*, 22725–22731. [CrossRef] [PubMed]
9. Li, D.; Chen, J.; Sun, T.; Zhang, Y.; Xu, J.; Li, W.; Chen, K. Enhanced subband light emission from Si quantum dots/SiO_2 multilayers via phosphorus and boron co-doping. *Opt. Express* **2022**, *30*, 12308–12315. [CrossRef] [PubMed]
10. Lin, G.R.; Pai, Y.H.; Lin, C.T.; Chen, C.C. Comparison on the electroluminescence of Si-rich SiN_x and SiO_x based light-emitting diodes. *Appl. Phys. Lett.* **2010**, *96*, 263514. [CrossRef]
11. Wang, F.; Li, N.; Jin, L.; Yang, D.; Que, D. Reduction of the efficiency droop in silicon nitride light-emitting devices by localized surface plasmons. *Appl. Phys. Lett.* **2013**, *102*, 081108. [CrossRef]
12. Huh, C.; Kim, B.K.; Park, B.-J.; Jang, E.-H.; Kim, S.-H. Enhancement in electron transport and light emission efficiency of a Si nanocrystal light-emitting diode by a SiCN/SiC superlattice structure. *Nanoscale Res. Lett.* **2013**, *8*, 14. [CrossRef] [PubMed]
13. Zhang, Y.; Zhang, C.; Li, S.; Dai, X.; Ma, X.; Gao, R.; Zhou, W.; Lu, M. Enhancing light emission of Si nanocrystals by means of high-pressure hydrogenation. *Opt. Express* **2020**, *28*, 23320–23328. [CrossRef] [PubMed]
14. Li, Q.; Luo, T.Y.; Zhou, M.; Abroshan, H.; Huang, J.; Kim, H.J.; Rosi, N.L.; Shao, Z.; Jin, R. Silicon Nanoparticles with Surface Nitrogen: 90% Quantum Yield with Narrow Luminescence Bandwidth and the Ligand Structure Based Energy Law. *ACS Nano* **2016**, *10*, 8385–8393. [CrossRef] [PubMed]
15. Molinari, M.; Rinnert, H.; Vergnat, M. Improvement of the photoluminescence properties in a-SiNx films by introduction of hydrogen. *Appl. Phys. Lett.* **2001**, *79*, 2172. [CrossRef]
16. Huang, R.; Song, J.; Wang, X.; Guo, Y.Q.; Song, C.; Zheng, Z.H.; Wu, X.L.; Chu, P.K. Origin of strong white electroluminescence from dense Si nanodots embedded in silicon nitride. *Opt. Lett.* **2012**, *37*, 692–694. [CrossRef] [PubMed]
17. Haberl, B.; Bogle, S.N.; Li, T.; McKerracher, I.; Ruffell, S.; Munroe, P.; Williams, J.S.; Abelson, J.R.; Bradby, J.E. Unexpected short- and medium-range atomic structure of sputtered amorphous silicon upon thermal annealing. *J. Appl. Phys.* **2011**, *110*, 096104. [CrossRef]
18. Rui, Y.; Chen, D.; Xu, J.; Zhang, Y.; Yang, L.; Mei, J.; Ma, Z.; Cen, Z.; Li, W.; Xu, L.; et al. Hydrogen-induced recovery of photoluminescence from annealed a-Si:H/a-SiO_2 multilayers. *J. Appl. Phys.* **2005**, *98*, 033532. [CrossRef]
19. Ren, Y.; Weber, K.J.; Nursam, N.M.; Wang, D. Effect of deposition conditions and thermal annealing on the charge trapping properties of SiNx films. *Appl. Phys. Lett.* **2010**, *97*, 202907. [CrossRef]
20. Lin, Z.; Huang, R.; Song, J.; Guo, Y.; Lin, Z.; Zhang, Y.; Xia, L.; Zhang, W.; Li, H.; Song, C.; et al. Engineering $CsPbBr_3$ quantum dots with efficient luminescence and stability by damage-free encapsulation with a-SiCx:H. *J. Lumin.* **2021**, *236*, 118086. [CrossRef]